LA-14383

High-Precision Gamma-Ray Total Cross-Section Measurements between 3.45 and 12 MeV

Los Alamos
NATIONAL LABORATORY
EST. 1943

Edited by Mable Amador, Group IRM-CAS.
Photocomposition by Deidre´ A. Plumlee, Group IRM-CAS.

Los Alamos National Laboratory, an affirmative action/ equal opportunity employer, is operated by Los Alamos National Security, LLC, for the National Nuclear Security Administration of the U.S. Department of Energy under contract DE-AC52-06NA25396.

LA-14383
Issued: December 2008

High-Precision Gamma-Ray Total Cross-Section Measurements between 3.45 and 12 MeV

Christen M. Frankle
Calvin E. Moss

Los Alamos
NATIONAL LABORATORY
EST. 1943

This page left blank intentionally.

High-Precision Gamma-Ray Total Cross-Section Measurements between 3.45 and 12 MeV

by

Christen M. Frankle and Calvin E. Moss

ABSTRACT

A Compton-backscatter capability has recently become available at the Duke University Free Electron Laser Laboratory. This capability allows one to produce high fluxes of tunable, nearly monoenergetic gamma rays. Using these gamma-ray beams, we have made high-precision (~0.5%) measurements of the gamma-ray total cross section at 3.45, 4, 5, 6, 8, 10, and 12 MeV. The nuclei measured were Be, C, Cu, Ta, W, Pb, and U.

INTRODUCTION

The motivation for these measurements is the need for the stockpile stewardship program to be able to quantitatively measure density profiles from radiographs. In particular, the radiographs of most interest are of shock-loaded systems that are taken using high-energy flash x-ray machines (e.g., PHERMEX and DAHRT). Such quantitative measurements of very high-density systems currently have large errors because of the fact that cross sections essentially have not previously been measured in the energy range above ~2.5 MeV. All cross sections currently used in radiographic analysis are theoretical predictions with estimated errors in the 2%–3% range. It should also be noted that the theoretical evaluations do not include photonuclear reactions, which become increasingly important at higher energies. Although these errors might seem small when propagated through the standard transmission equation, $T = e^{-n\sigma}$, where $n\sigma$ is large, the error on the derived n is significant. (Here n is the areal density in at/b and σ is the cross section in b.) We were therefore tasked with measurement of the cross section at energies of 3.45, 4, 5, 6, 8, 10, 12, and 14 MeV to $\delta\sigma/\sigma<0.5\%$ and $\delta E/E<1\%$ FWHM. This part of the measurement campaign is nearly complete (approximately one week of beam is still needed) for the initial set of specified materials (Be, C, Cu, Ta, W, Pb, and depleted uranium). We are issuing this interim report in order to make the data that have been taken to date available to the program while we await resumption of funding to complete the measurements. We have also performed similar measurements in the energy range of 0.847 to 3.451 MeV using a ^{56}Co radioactive source. These data will be reported in a separate paper.

The accurate knowledge of the gamma-ray total cross sections is important for almost any application where gamma rays are used as a tool, whether it be radiography, medical treatments, gauging, etc. Equally as important is the need for the same accurate data when gamma-ray shielding is to be designed.[1] Over the years many compendia of calculated values have been published, see for example References [2, 3, 4, 5, 6], and [7]. Variations between the different compendia typically run in the range of one to three percent in the energy range that we are

interested in. This is acknowledged to be the approximate uncertainty on the calculated total gamma-ray cross section.[8]

Experimental data on the gamma-ray total cross section has been profuse in the region up to several hundred keV. However, data in the region of several MeV and above is quite scarce. In general, most data have been limited to the highest energy gamma-ray that could reasonably be obtained using a radioactive source. Typically this has meant ^{24}Na which has a gamma-ray at 2.75 MeV.[9] However, a small amount of data has been published in the range of six to eight MeV[10, 11] using secondary gamma rays generated from neutron capture reactions.

It is well known that the narrow beam transmission of gamma rays follows the simple relation

$$I = I_0 e^{-n\sigma} \ , \qquad (1)$$

where I_0 is the incident intensity, I is the transmitted intensity, n is the target thickness in at/b, and σ is the total cross section. In certain applications where quantitative information on the thickness of a material measured by gamma-ray absorption is desired, the current level of accuracy in the published cross sections is insufficient. In particular, if the material to be measured is many path-lengths thick, then small variations in the cross section are amplified through the exponential behavior (Eq. 1) of the absorption to give large differences in the transmission. It was therefore our objective to measure the total cross sections to a precision of ~0.5% in order to improve the ability to make quantitative material thickness measurements.

Measurements of this precision have only been possible since the recent construction of a Compton-backscatter facility at the Duke University Free Election Laser Laboratory (DFELL). This facility is unique in the ability to provide a high flux (~10^6 γ/s), tunable, essentially monoenergetic gamma-ray beam of any energy between approximately 3 and 70 MeV. In addition, the gamma-ray beam is essentially similar to the laser beam produced by the DFELL electron storage ring and optical cavity. Therefore, we are provided a nearly perfect narrow beam geometry with collimation only required to limit the beam energy spread. We have chosen to make our measurements in the range of approximately 3 to 15 MeV, which is of particular interest to the quantitative interpretation of flash radiographs taken using bremstraalung-spectrum photons from pulsed electron linear accelerators.

In the following section, we present details of the experimental technique. A discussion of the DFELL facility is also included. The analysis methods and resulting cross sections are given Section III. Finally, in Section IV we summarize and compare the measured results with several recent evaluations.

EXPERIMENT

Facility

The DFELL relies upon Compton backscattering techniques to generate the gamma-ray beams used in this experiment. The collision of relativistic electrons and low energy photons produces gamma rays that are strongly peaked in the direction of the incident electrons. When $E_e / m_e c^2 >> 1$ the energy of the outgoing gamma rays is given by

$$E_\gamma \cong \frac{4\gamma^2 E_{ph}}{1 + (\gamma\theta)^2 + 4\gamma \frac{E_{ph}}{m_e c^2}}, \qquad (2)$$

where $\gamma = E_e / m_e c^2$, E_{ph} is the incident photon energy, and θ is the angle between the incident electrons and the outgoing gamma rays.[12] This form means that the maximum beam energy is at $\theta = 0$ and drops off for $\theta \neq 0$. This gives the beam two features. First, for a perfect electron beam, the energy resolution of the beam can be arbitrarily selected by defining a θ_{max} with a collimation system. Second, the beam will always have a characteristic low-energy tail. In practice, the electron beam is not perfect; it has both spatial and energy dispersion, and the actual energy resolution of the beam is defined by the combination of the electron beam dispersion and the beam collimation.

The layout of the DFELL is illustrated schematically in Figure 1. Electrons are injected into the ring by a linear accelerator operating at 270 MeV. Once the ring is filled with the desired number of electrons, injection is stopped and the ring energy can be ramped up to a maximum electron energy of 1.1 GeV. During the course of this experiment, electron-beam energies between 300 and 600 MeV were used to obtain the desired gamma-ray energies. Broadband, tunable mirrors covering most of the UV and visible spectrum were used in the optical klystron, which allowed all of the gamma-ray energies to be achieved with a single set of mirrors. Detailed descriptions of the DFELL storage ring and optical klystron have been published elsewhere.[13, 14]

The gamma-ray beam was transported approximately 100 m from the electron-photon collision point in vacuum. At that point, a 5-mm diameter, 10-cm thick Pb collimator was used to define the beam-energy spread. The beam-energy spread was held to less than 1% FWHM in all cases.

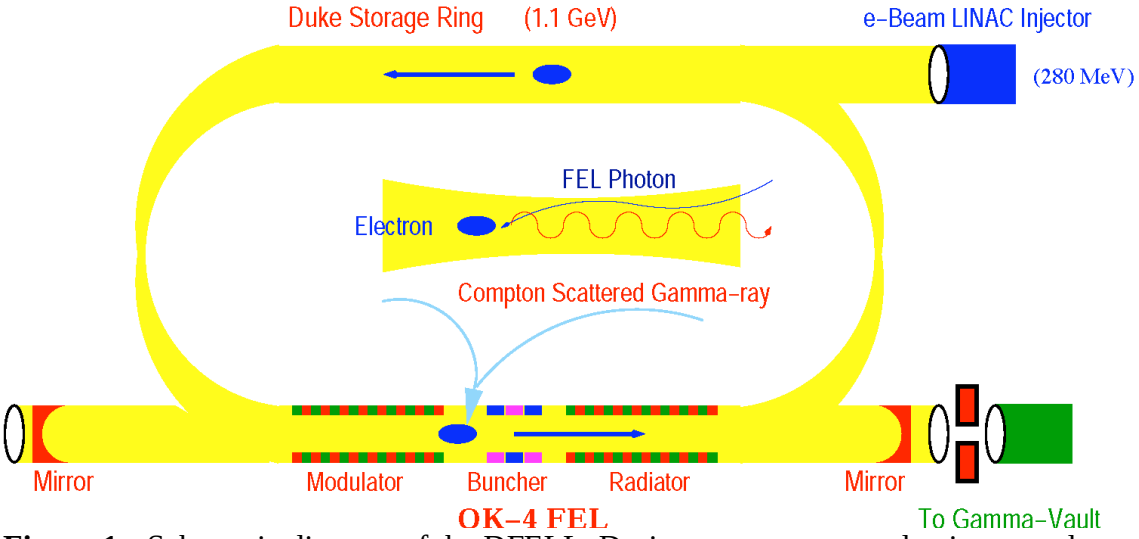

Figure 1. Schematic diagram of the DFELL. During gamma-ray production two electron bunches are in the ring, separated by 180°. Both bunches contribute to lasing and gamma-ray production.

Absorption Measurement

In concept, the measurement of the gamma-ray total cross section involves a "sample-in/sample-out" process. The "sample-out" case is the measurement of the beam intensity without a sample, corresponding to I_0 of Equation (1). The "sample-in" case is the measurement of the beam intensity with a sample of known thickness n in place, corresponding to I in Equation (1). Then, by simple rearrangement of Equation (1) in to the form

$$\sigma = -\frac{1}{n}\ln\left(\frac{I}{I_0}\right), \qquad (3)$$

the cross section σ is obtained. In practice, however, several additional factors that influence the measurement are present. Unlike a long-lived radioactive source, the gamma-ray flux is not constant. The electron bunches in the storage ring have a half-life on the order of an hour, causing a slow decay of the gamma-ray flux with time. In addition, various instabilities in the electronic control systems of the DFELL may cause other variations in the gamma-ray flux because of changes in electron-beam properties on a shorter time scale. Therefore, it becomes necessary to monitor the beam flux as a function of time. Also, no detector system is without losses ("dead time"), something important to account for in this experiment because the counting rates in the "sample-in" and "sample-out" cases are quite different. Finally, the detectors used in this experiment are not only sensitive to beam gamma rays but to other gamma rays that may also be present in the experimental area. Therefore, these background gamma rays must also be accounted for. Incorporating these factors into Eq. (3) yield the form

$$\sigma = -\frac{1}{n}\ln\left(\frac{\left(\frac{A}{t_L}\right)\left(\frac{1}{M - M_{bkg}}\right)}{\left(\frac{A_0}{t_{L_0}}\right)\left(\frac{1}{M_0 - M_{bkg_0}}\right)}\right), \qquad (4)$$

where A represents the net counts in the detector placed after the sample, t_L represents the "live-time" associated with the net counts A, and M represents the counts per second in the beam monitor detector. The subscript 0 indicates the "sample-out" measurement.

Our implementation of this is shown in a schematic beam line diagram in Figure 2. Because of the construction of a new building at DFELL and scheduling difficulties, this experiment was performed in two phases with slightly different beam-line configurations. The Cu and W data between 3.45 and 12 MeV was taken with the configuration as shown and a source to detector distance of 2 m. All other data were taken without the post collimator and with a source to detector distance of 5.7 m. A 3-mm defining collimator was used originally. This was later changed to a 5-mm collimator when it was found that the 5-mm collimator caused no additional loss of beam-energy resolution.

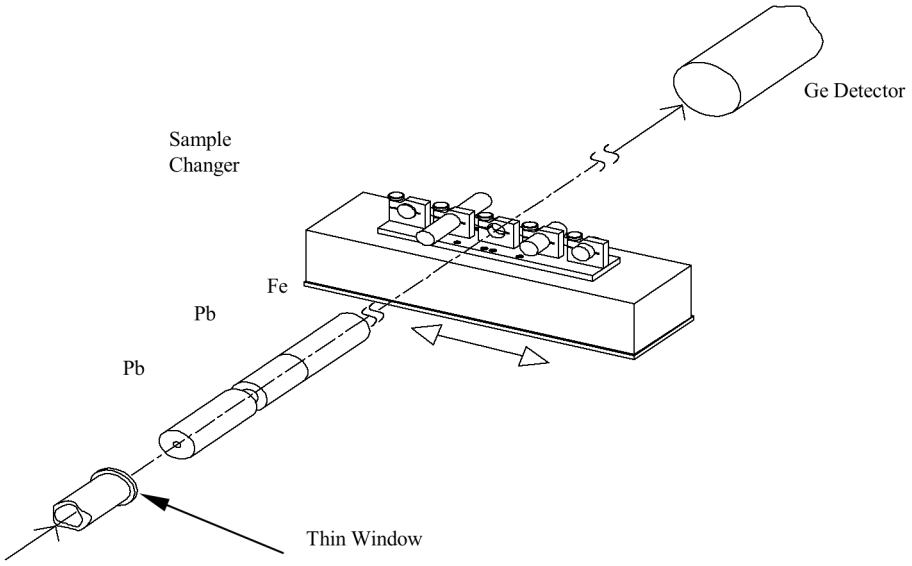

Figure 2. Schematic diagram of the beam line apparatus. The gamma-ray beam passes out of the evacuated beam pipe, through a thin crystalline window to be collimated and monitored before passing through the sample and onto the HPGe detector.

The basic assumption behind the "sample-in/sample-out" technique is that only gamma rays that have not interacted in the sample are recorded in the detector. In this experiment we have used a high-purity germanium (HPGe) detector with a relative efficiency of 128%. The resolution of the detector is approximately 0.05% in the energy region of interest, significantly smaller than the energy resolution of the beam. The net counts obtained are only those that are recorded in the detector full-energy peak. Therefore, any gamma ray that interacts in the sample but loses more energy than the beam energy spread is automatically rejected. The more difficult issue is a

gamma ray that scatters in the sample, does not lose more energy than the beam energy spread, and ends up in the detector. Such gamma rays are dealt with by minimizing the available solid angle. In the latter phase of this experiment, we have placed the detector 5.7 m downstream from the sample position. In this position, the cone angle available for scattering is 0.02 degrees. Even in the worst case of U at 3.45 MeV, the coherent part of the cross section is only 0.8% of the total; therefore, any corrections would be in the μb range, far smaller than the other errors present in the experiment. In the earlier phase of the experiment where the source to detector distance was only 2 m, a maximum correction of 18 mb had to be applied to the W data, as discussed below.

The beam monitor was a fast plastic scintillator 3 mm thick. The scintillator was approximately 5 cm by 5 cm and fully covered the beam. The rise time of the output signal from the photomultiplier tube was approximately 2 ns. This signal was then discriminated, and a 10 ns fast NIM pulse was used as input to the beam monitor scalar.

In order to assist us in the identification of possible systematic errors in the data, we chose to run more than one sample thickness. For most of the samples we used four thicknesses, corresponding to approximately one-half, one, two, and four path lengths. These samples were mounted on a computer-controlled mechanical sample positioner that was equipped to hold the four sample thicknesses plus a blank, "sample-out" position. The sample positioner is an industrial single-axis linear motor. The motor has a position reproduceability of better than 0.001 cm. The sequence of sample changes was one-half path length, four path lengths, blank, two path lengths, one path length, and repeat.

All of the samples were machined right circular cylinders 2.54 cm in diameter. Except for the Be and C samples, four lengths were fabricated for each material corresponding to approximately one-half, one, two, and four path lengths. Because of the fact of the low Z and low density of Be and C, the thickest samples would have been excessively long for those cases; therefore three samples were fabricated of C and two of Be, corresponding to one-half, one, and two path lengths for the C and one-half and one path length for the Be. All sample material was of 99.99% or better chemical purity. The measured length and density of each sample is given in Table I. The uranium samples are depleted uranium containing a nominal 0.21% ^{235}U.

The process of acquiring data was fully automated under computer control. The computer was first linked through RS232 to the sample positioner. Once the feedback from the linear motor indicated that it was in the proper position, the computer then started a one-minute acquisition of data using an ORTEC multichannel analyzer (MCA). The MCA was set to collect 16,384 channels of data with a nominal dispersion of 1 keV per channel. Although the MCA was acquiring data a 100 MHz CAMAC scalar was also recording the number of beam monitor pulses and separate clock output. There was an approximately 0.1 s difference in acquisition time of the MCA and the scalar because of delays in the software. By allowing the MCA and scalar to have their own clocks this difference was properly accounted for. During the time the data from the MCA and scalar were saved to disk the sample positioner moved to the next position. Both the MCA and the CAMAC crate were linked to the computer through ethernet. A complete cycle through all five sample positions took a little over five minutes because of various overheads.

Table I: Physical Data of the Samples			
Sample	**Length (cm)**	**Density (g/cm^3)**	**Thickness (at/b)**
Be-1	12.802 ± 0.003	1.8485 ± 0.0006	1.5815 ± 0.0006
Be-2	25.644 ± 0.004	1.8486± 0.0006	3.1628 ± 0.0008
C-1	7.653 ± 0.003	1.835 ± 0.009	0.704 ± 0.004
C-2	15.288 ± 0.003	1.844± 0.009	1.414 ± 0.007
C-3	30.81 ± 0.03	1.840 ± 0.009	2.843 ± 0.014
Cu-1	1.793 ± 0.003	8.93 ± 0.02	0.1517 ± 0.0005
Cu-2	3.584 ± 0.003	8.93± 0.02	0.3034 ± 0.0007
Cu-3	7.178 ± 0.003	8.935 ± 0.018	0.6079 ± 0.0013
Cu-4	14.351 ± 0.003	8.936 ± 0.018	1.216 ± 0.003
Ta-1	0.6741 ± 0.0005	16.63 ± 0.13	0.0373 ± 0.0003
Ta-2	1.4430 ± 0.0005	16.66 ± 0.06	0.0800 ± 0.0003
Ta-3	2.8791 ± 0.0013	16.68 ± 0.03	0.1598 ± 0.0003
Ta-4	5.7645 ± 0.0013	16.672 ± 0.016	0.3199 ± 0.0003
W-1	0.6129 ± 0.0005	19.18 ± 0.17	0.0385 ± 0.0003
W-2	1.2365 ± 0.0005	19.15 ± 0.09	0.0776 ± 0.0004
W-3	2.4684 ± 0.0005	19.19± 0.04	0.1552 ± 0.0003
W-4	4.9416 ± 0.0013	19.19 ± 0.02	0.3107 ± 0.0003
Pb-1	1.0058 ± 0.0003	11.35 ± 0.06	0.0332 ± 0.0002
Pb-2	2.0104 ± 0.0003	11.34 ± 0.03	0.0663 ± 0.0002
Pb-3	4.0229 ± 0.0005	11.339 ± 0.015	0.1326 ± 0.0002
Pb-4	8.0462 ± 0.0010	11.342 ± 0.008	0.2653 ± 0.0002
U-1	0.650 ± 0.004	19.08 ± 0.16	0.0314 ± 0.0003
U-2	1.270 ± 0.004	19.07 ± 0.08	0.0613 ± 0.0003
U-3	2.535 ± 0.004	19.04 ± 0.04	0.1221 ± 0.0003
U-4	5.088 ± 0.008	19.03 ± 0.02	0.2450 ± 0.0005

During the initial measurement sequence of the campaign, we used an analog MCA. It was found that the analog MCA was limited to a few kHz maximum counting rate. At that rate, the beam had to be detuned so as not to overwhelm the MCA. Subsequently, we purchased a digital MCA, which by utilizing digital signal processing is able to handle about three times the counting rate of the analog MCA. After a complete set of data was taken, it was discovered during the analysis that the dead time reported by the digital MCA could not be properly reconciled for high energy (above ~10 MeV) beams. This led to an extensive investigation into the behavior of the MCA. It turns out that essentially all gamma-ray pulses cause some low-level electronic “ringing” in the system. This is normally rejected by an internal discriminator. However, we found that in the case of large pulses, the level of the ringing can exceed the discriminator level that causes one or more additional triggers of the dead-time clock but did not result in additional counts in the spectrum. Therefore, all of the data taken with the digital MCA at 12 and 14 MeV had to be rejected. It is possible that the 10-MeV data also have a small amount of error because of this effect. We plan to recheck the 10-MeV data when we return to DFELL to redo the 12 and 14 MeV data, however, we do report below the 10 MeV data as it stands. Users of these data should be cautioned that the 10 MeV data on Be, C, Ta, Pb, and U *may* have a systematic error of up to ~0.3% because of this effect. The 10 and 12 MeV data on Cu and W were taken with the analog MCA and does not suffer from this problem.

DATA ANALYSIS AND RESULTS

The operational sequence of the DFELL was such that the storage ring would be injected and ramped, lasing would be achieved, and gamma rays would be produced. The ring and optical klystron would then be left in this essentially steady state mode for about 50 to 90 minutes. As discussed above, the number of electrons in the ring would slowly decay during this time. Once the number of electrons in the ring had decayed to 30% to 40% of the initial value, it was advantageous to reinject. Therefore, the data from one injection sequence were conveniently combined into a "run." A single run typically had 10 to 15 complete sample cycles in it. In all cases, we collected at least two runs per target/energy pair for intercomparison purposes.

The first step in the analysis was to energy-calibrate the spectrum to obtain the exact energy of the beam. The open beam data was used for calibration purposes. All available background lines in the spectrum were first identified. These were primarily from the ^{232}Th decay series, plus ^{40}K. Usable lines ranged from 0.583 MeV at the low energy end to 2.614 MeV at the high-energy end. A minimum of four lines was used to establish a quadratic polynomial fit for the channel-energy correlation. We also required that the fitted curve be such that the separation between the full-energy and first escape peaks be exactly 0.511 MeV. A full spectrum for a 6-MeV beam is shown in Figure 3. The data for this experiment were obtained in three separate campaigns. After the first campaign, which produced most of the Cu and W data, it was recognized that this energy calibration procedure would benefit from a high-energy tie point. Therefore, for all remaining data, the nights when the beam was off were used to obtain gamma-ray spectra from a moderated AmBe neutron source. The 10.829 MeV neutron capture line from ^{14}N and/or the 10.196 MeV sum peak from neutron capture on ^{73}Ge were used in addition to the previously described procedure.

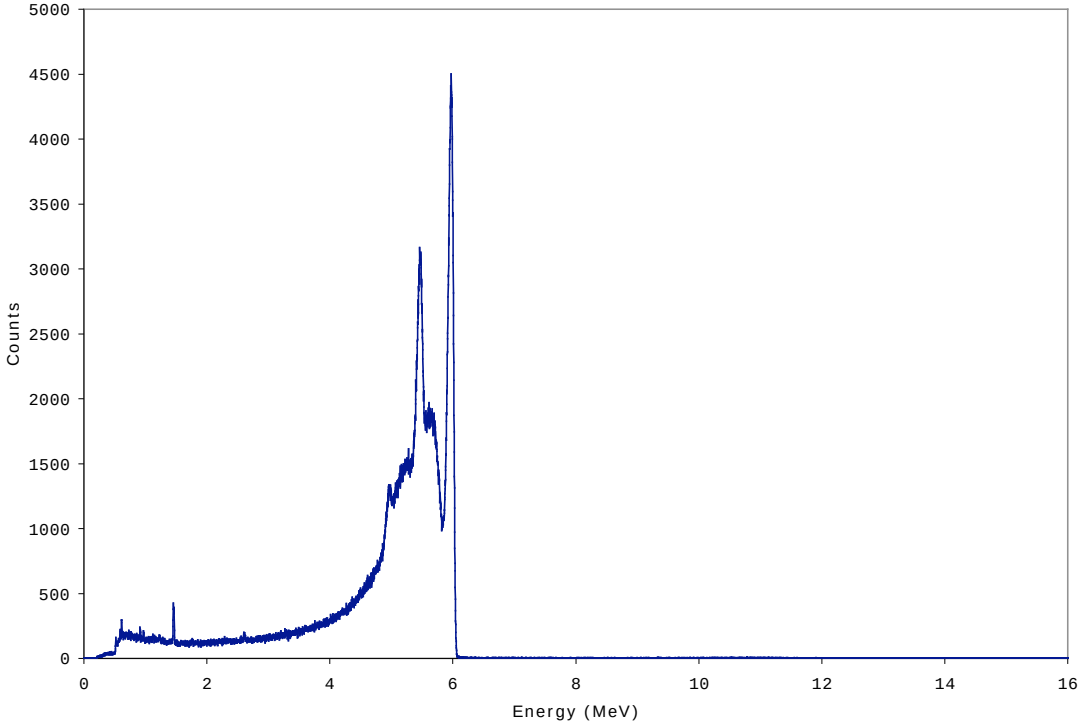

Figure 3. Gamma-ray energy spectrum from a 6 MeV gamma-ray beam in the open beam configuration.

Once the energy calibration was established, then the region between the high-energy side of the first escape peak and the high-energy side of the full-energy peak was fit. The software package PeakFit from the SPSS Company was used for the fitting. A Gaussian with an additional Gaussian tail on the low energy side was used as the functional form of the full energy peak and a Compton edge form was used for the Compton edge of the full energy peak. An example fit is shown in Figure 4. From this fit, a FWHM and net area were obtained for the full energy peak. This process was then repeated for each of the other four sample positions.

For each sample position, the live-time used was as recorded by the MCA. The beam monitor count rate was computed from the scalars that recorded the number of beam monitor pulses and the number of beam-monitor clock pulses. The beam-monitor background count rate was found by running background measurements during the nights when the accelerator was off. These data, along with the sample thicknesses, were used in Equation 4 to compute a cross section for each of the four sample thicknesses for each target/energy/run combination. An overall cross section for each run was then computed by taking the weighted average of the cross sections for all the sample thicknesses. Finally, a weighted average was taken across all of the runs to obtain an overall value for the cross section. In addition, a weighted average cross section was computed across each sample thickness to examine for possible systematic deviation from the overall computed cross section.

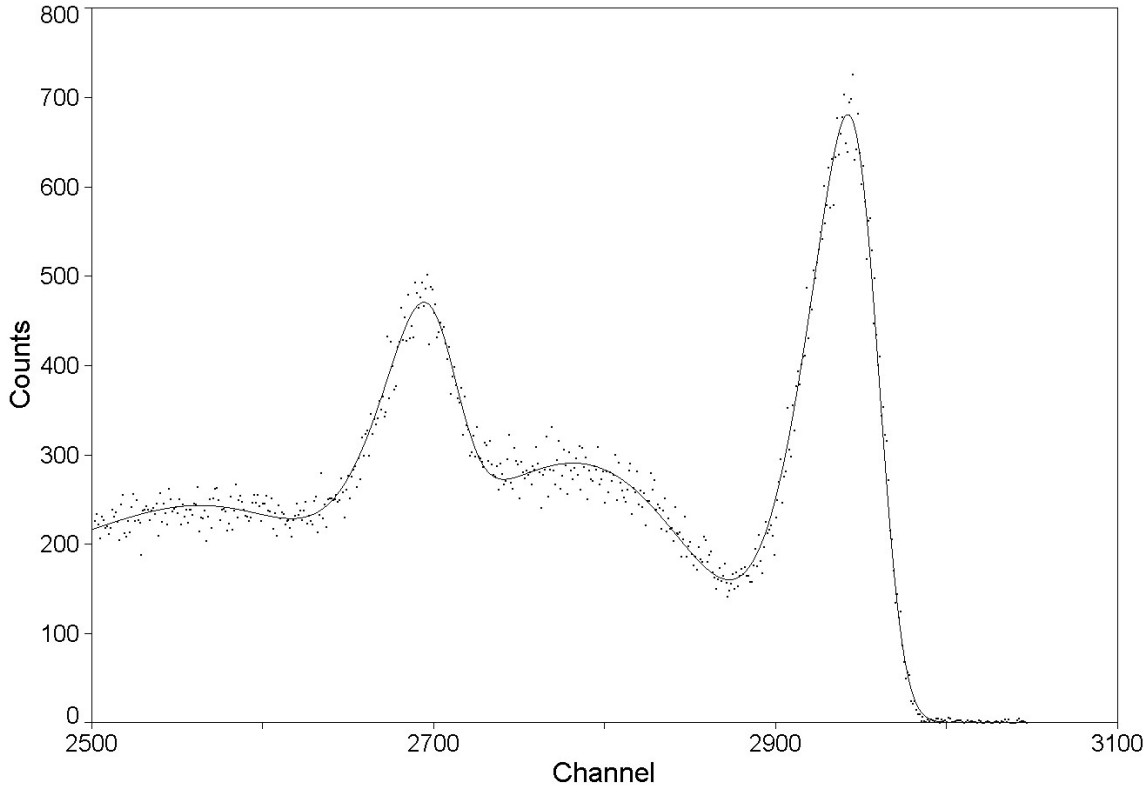

Figure 4. Fit to one run with a two-path-length thickness of Cu and a 6 MeV beam.

As mentioned earlier, data that were acquired during the first campaign (most of the Cu and W data) had a significantly smaller target-to-detector distance. The result of this was the need for a small correction to the measured cross section to account for gamma rays that coherently scattered and were detected by the HPGe detector. In order to perform this correction, we first consider the probability of a coherent scattering event occuring at a depth z in the sample,

$$dY = \frac{n}{D} e^{-n\sigma_t z/D} \sigma_c dz \,. \qquad \textbf{(5)}$$

However, not all gamma rays will make it out of the sample; therefore, the total probability then becomes

$$Y = \int_0^D \frac{n}{D} e^{-n\sigma_t z/D} e^{-n\sigma_t (D-z)/D} dz \sigma_c \,. \qquad \textbf{(6)}$$

From this, a corrected transmission can then be computed as

$$T_{corr} = T_{meas}\left(1 - Y\right). \qquad \textbf{(7)}$$

The corrected transmission is then used to compute the cross section. This correction was needed only for the initial Cu and W measurements where the detector was limited to 2 m from the samples. The maximum correction, applied at 3.45 MeV for the W samples, was 18 mb.

In successive measurement campaigns a few data points on Cu were repeated to check for consistency with data taken during earlier campaigns. In no case were any repeated measurements different by more than 1.2 sigma, and most were well within one sigma. The repeated data points are shown in Table II.

Table II. Repeated Cross-Section Measurements on Cu

Energy (MeV)	σ (b)	Energy (MeV)	σ (b)
3.447 ± 0.015	3.640 ± 0.010	3.446 ± 0.017	3.644 ± 0.007
5.97 ± 0.02	3.255 ± 0.008	5.99 ± 0.04	3.253 ± 0.016
8.01 ± 0.04	3.206 ± 0.009	7.98 ± 0.03	3.218 ± 0.012

The results of this analysis are given in Table III for Be, Table IV for C, Table V for Cu, Table VI for Ta, Table VII for W, Table VIII for Pb, and Table IX for U. Note that the errors quoted are one sigma. For those data points that had a repeat measurement, the values listed in the tables are the weighted averages of all measurements.

Table III. Measured Cross Sections for Be

Energy (MeV)	σ (b)
3.443.± 0.016	0.4354 ± 0.0015
4.007 ± 0.014	0.3983 ± 0.0013
4.98 ± 0.02	0.3544 ± 0.0013
6.01 ± 0.02	0.3158 ± 0.0014
7.98 ± 0.03	0.2696 ± 0.0016
10.01 ± 0.04	0.2438 ± 0.0014

Table IV: Measured Cross Sections for C

Energy (MeV)	σ (b)
3.444 ± 0.014	0.656 ± 0.002
4.003 ± 0.014	0.604 ± 0.002
4.99 ± 0.02	0.535 ± 0.002
5.99 ± 0.02	0.492 ± 0.002
7.98 ± 0.03	0.427 ± 0.002
10.01 ± 0.04	0.3882 ± 0.0019

Table V. Measured Cross Sections for Cu

Energy (MeV)	σ (b)
3.446 ± 0.017	3.643 ± 0.006
4.01 ± 0.02	3.522 ± 0.007
5.01 ± 0.03	3.355 ± 0.009
5.98 ± 0.04	3.255 ± 0.007
8.01 ± 0.04	3.210 ±0.007
9.99 ± 0.03	3.307 ± 0.016
11.96 ± 0.03	3.34 ± 0.03

Table VI. Measured Cross Sections for Ta

Energy (MeV)	σ (b)
3.445 ± 0.013	12.01 ± 0.03
4.001 ± 0.014	12.01 ± 0.03
5.00 ± 0.02	12.29 ± 0.03
5.98 ± 0.02	12.59 ± 0.03
8.03 ± 0.04	13.27 ± 0.03
10.00 ± 0.04	14.23 ± 0.03

Table VII. Measured Cross sections for W

Energy (MeV)	σ (b)
3.454 ± 0.018	12.18 ± 0.04
3.965 ± 0.018	12.21 ± 0.03
4.97 ± 0.02	12.29 ± 0.03
5.97 ± 0.03	12.66 ± 0.03
7.98 ± 0.03	13.59 ± 0.03
9.91 ± 0.04	14.55 ± 0.06
11.83 ± 0.04	15.10 ± 0.11

Table VIII. Measured Cross Sections for Pb

Energy (MeV)	σ (b)
3.449 ± 0.014	14.34 ± 0.03
4.005 ± 0.014	14.28 ± 0.03
5.003 ± 0.019	14.66 ± 0.04
5.99 ± 0.02	15.09 ± 0.04
8.01 ± 0.04	15.86 ± 0.04
10.00 ± 0.04	17.16 ± 0.04

Table IX. Measured Cross Sections for U

Energy (MeV)	σ (b)
3.448 ± 0.014	17.18 ± 0.05
4.008 ± 0.014	17.20 ± 0.05
4.985 ± 0.019	17.46 ± 0.04
5.97 ±0.03	18.20 ± 0.05
8.02 ± 0.03	19.27 ± 0.04
10.01± 0.04	20.58 ± 0.06

SUMMARY

We have measured the gamma-ray total cross section of Be, C, Cu, Ta, W, Pb, and U in the energy range of 3.45 to 12 MeV. Measurement accuracies were generally ~0.3%. It is important to point out that when comparing these data to evaluations, photonuclear contributions are not normally included in evaluations. Photonuclear contributions become increasingly important at higher energies. These data are true total cross sections, which include all physical processes.

---

[1] J.H. Hubbell and M.J. Berger, Engineering Compendium on Radiation Shielding, edited by R.G. Jaeger (Springer, Berlin, 1968) pp.167–202.
[2] J.H.Hubbell, Natl. Stand. Ref. Data Ser. 29 (1969).
[3] W.H. McMaster, N.K. DelGrande, J.H. Mallett, and J.H. Hubbell, Lawrence Livermore National Laboratory Report UCRL-50174, (1969).
[4] E. Storm and H.I. Israel, Nuclear Data Tables A7, 565 (1970).
[5] E.F. Plechaty, D.E. Cullen, and R.J. Howerton, Lawrence Livermore National Laboratory Report UCRL-50400, (1981).
[6] J.H. Hubbell, Int. J. Appl. Radiat. Isotopes 33, 1269 (1982).
[7] D.E. Cullen, J.H. Hubbell, and L. Kissel, Lawrence Livermore National Laboratory Report UCRL-50400, rev 5., (1997).
[8] J.H. Hubbell, X-Ray Spectrom. 28, 215 (1999).
[9] A.L. Conner, H.F. Atwater, E.H. Plassmann, and J.H. McCrary, Phys. Rev. A1, 539 (1970).
[10] R. Moreh, D.Salzmann, and Y. Wand, Phys. Lett. 30B, 536 (1969).
[11] R. Moreh and Y.Wand, Nucl. Phys. A252, 423 (1975).
[12] V.N. Litvinenko, et al., Phys. Rev. Lett. 78, 4569 (1997).
[13] Y. Wu, et al., Nucl. Instrum. Methods A375, 74 (1996).
[14] V.N. Litvinenko, et al., Nucl. Instrum. Methods A375, 46 (1996).

This page left blank intentionally.


Los Alamos
NATIONAL LABORATORY
EST. 1943